

Solution Structure of RING Finger-like Domain of Retinoblastoma-binding Protein-6 (RBBP6) Suggests It Functions as a U-box^{*S}

Received for publication, December 31, 2010, and in revised form, November 8, 2011. Published, JBC Papers in Press, November 30, 2011, DOI 10.1074/jbc.M110.217059

Mautin A. Kappo[‡], Eiso AB[§], Faqeer Hassem[‡], R. Andrew Atkinson^{¶1}, Andrew Faro[‡], Victor Muleya[‡], Takalani Mulaudzi[‡], John O. Poole[‡], Jean M. McKenzie^{||}, Moredreck Chibi[‡], Joanna C. Moolman-Smook^{**}, D. Jasper G. Rees[‡], and David J. R. Pugh^{‡1,2}

From the [‡]Biotechnology Department, University of the Western Cape, Bellville 7535, South Africa, [§]ZoBio BV, Einsteinweg 55, 2333 CC Leiden, The Netherlands, the [¶]Institut de Génétique et de Biologie Moléculaire et Cellulaire, 1 rue Laurent Fries, 67404 Illkirch Cedex, France, the ^{||}NMR Laboratory, Central Analytical Facility, University of Stellenbosch, Private Bag S1, Matieland 7602, South Africa, and the ^{**}Health Sciences Faculty, University of Stellenbosch, Tygerberg 7505, South Africa

Background: U-box-containing proteins cooperate with chaperones in ubiquitinating irreversibly unfolded proteins.

Results: Retinoblastoma binding protein-6 (RBBP6) contains a zinc-binding U-box-like domain and interacts directly with chaperones.

Conclusion: RBBP6 may play a role in protein quality control.

Significance: U-boxes should be classified in terms of their interaction with chaperones and not their zinc binding properties.

Retinoblastoma-binding protein-6 (RBBP6) plays a facilitating role, through its RING finger-like domain, in the ubiquitination of p53 by Hdm2 that is suggestive of E4-like activity. Although the presence of eight conserved cysteine residues makes it highly probable that the RING finger-like domain coordinates two zinc ions, analysis of the primary sequence suggests an alternative classification as a member of the U-box family, the members of which do not bind zinc ions. We show here that despite binding two zinc ions, the domain adopts a homodimeric structure highly similar to those of a number of U-boxes. Zinc ions could be replaced by cadmium ions without significantly disrupting the structure or the stability of the domain, although the rate of substitution was an order of magnitude slower than any previous measurement, suggesting that the structure is particularly stable, a conclusion supported by the high thermal stability of the domain. A hallmark of U-box-containing proteins is their association with chaperones, with which they cooperate in eliminating irretrievably unfolded proteins by tagging them for degradation by the proteasome. Using a yeast two-hybrid screen, we show that RBBP6 interacts with chaperones Hsp70 and Hsp40 through its N-terminal ubiquitin-like domain. Taken together with the structural similarities to U-box-containing proteins, our data suggest that RBBP6 plays a role in chaperone-mediated ubiquitination and possibly in protein quality control.

Retinoblastoma-binding protein-6 (RBBP6) is a multi-functional protein found ostensibly in all eukaryotes but not in bacteria, which is implicated in a diverse set of cellular functions, including mRNA metabolism (1–3), regulation of the cell cycle (4–8), tumorigenesis (9), and development (10, 11). It forms part of the pre-mRNA 3-end processing complex (3) in humans and the cleavage and polyadenylation factor complex in yeast (2) and has been shown to interact directly with tumor suppressors p53 and the retinoblastoma gene product (1, 13).

RBBP6 contains an N-terminal ubiquitin-like domain (14) and a cysteine-rich RING finger-like domain, through which it promotes the ubiquitination of p53 by Hdm2 in an E4-like manner (10). Also through its RING finger-like domain, RBBP6 interacts directly with the pro-proliferative transcription factor Y-box-binding protein-1 (YB-1), and overexpression of RBBP6 in cultured mammalian cells leads to suppression of YB-1 in a proteasome-dependent manner (15). Whether this represents an example of E4- or E3-like behavior has yet to be determined. However, because it down-regulates both the pro-apoptotic p53 and the anti-apoptotic YB-1, the effect of RBBP6 on tumorigenesis is likely to be highly complex.

The cysteine-rich domain of RBBP6 has been classified both as a RING finger, due to the presence of eight conserved cysteine residues, and as a U-box, due to a conserved pattern of hydrophobic residues (16). RING fingers are small domains, ~70 residues in length, that fold independently with the help of two Zn²⁺ ions. The ions are coordinated by four pairs of cysteine or histidine residues in a so-called “cross-braced” fashion, meaning that one of the ions is coordinated by the first and third Cys/His pairs and the other ion by the second and fourth Cys/His pairs. RING fingers are classified according to the pattern of zinc coordinating residues, with C3HC4 being the most common, although C3HHC3, C2H2C4, and C4C4 RING fingers are also found. The presence of eight conserved cysteine

* This work was supported in part by the National Research Foundation of South Africa and the Medical Research Council of South Africa.

^S This article contains supplemental Tables 1–3 and Figs. 1–5.

The atomic coordinates and structure factors (code 3ZTG) have been deposited in the Protein Data Bank, Research Collaboratory for Structural Bioinformatics, Rutgers University, New Brunswick, NJ (<http://www.rcsb.org/>).

¹ Recipient of grants from National Research Foundation of South Africa and the CNRS.

² Recipient of sabbatical funding from The Oppenheimer Memorial Trust. To whom correspondence should be addressed: Biotechnology Dept., University of the Western Cape, Private Bag X17, Bellville 7535, South Africa. Tel.: 27-21-959-2211; Fax: 27-21-959-1549; E-mail: dpugh@uwc.ac.za.

residues therefore suggests that RBBP6 contains a C4C4 RING finger domain binding two zinc ions.

RING fingers all share the same basic fold consisting of two large loops, each stabilized by a single zinc ion, lying parallel to an α -helix and together packing against a short three-stranded β -sheet. An identical fold is found in the U-box family, although there the coordination of zinc ions is replaced by a scaffold of salt bridges and hydrogen bonds (17). Most U-boxes and some RING fingers have been shown to form homodimers in solution, and in some cases dimerization has been shown to be required for ubiquitination activity (18, 19). Dimerization takes place along the β -sheet and is stabilized by interactions between the N and C termini of both monomers; the RING domains from the BRCA1/BARD1 heterodimer each contain N- and C-terminal helices that interact to form a 4-helix bundle. In the U-box domains from CHIP and PUB14, the N-terminal helices are replaced by structured loops that pack against and C-terminal helices, which constitute the bulk of the interface.

The primary function of RING fingers and U-boxes is to recruit the ubiquitin-conjugated E2 so that ubiquitin can be transferred from the E2 to the substrate, which in its turn is recruited by the substrate-binding domain of the E3. In addition to their characterization as “zinc-less RING fingers,” U-boxes were originally considered to be the hallmark of E4 ligases (also called elongation factors), which catalyze the addition of ubiquitin to pre-existing polyubiquitin chains but not to the substrate itself. However, many U-boxes have subsequently been shown to be capable of catalyzing polyubiquitination without the need for a separate initiating E3 ligase, rendering the association with E4 ligases problematic. More recently, U-boxes have become associated with chaperone-mediated ubiquitination and protein quality control (20). Many U-boxes have been shown to interact directly with chaperones or co-chaperones (21), the most well characterized being the C terminus of Hsp70 interacting protein (CHIP), which interacts with Hsp70 and Hsp90 through its tetratricopeptide domain, ubiquitinating unfolded proteins presented to it by Hsp70 (22–24). To resolve the question of whether RBBP6 contains a RING finger or a U-box domain, and to provide a structural framework for future interaction studies, we set out to determine the structure of the human domain using solution-state NMR spectroscopy.

EXPERIMENTAL PROCEDURES

Sequence Alignment—Sequences were aligned using Jalview (25). The supplemental Fig. 1 was generated using PFAAT (26).

Bacterial Expression and Purification—DNA sequences incorporating BamHI and XhoI restriction sites were amplified from a full-length cDNA clone of RBBP6 (15) and cloned into the corresponding sites of pGEX-6P-2 expression plasmids (GE Healthcare). ^{15}N , ^{13}C -Enriched GST fusion proteins were expressed as described previously (14), with the addition of 2 mM ZnSO_4 to the culture media following induction with isopropyl 1-thio- β -D-galactopyranoside. With the exception of the concentration series, all concentrations used for NMR analysis were in the range 1–2 mM.

Mass Spectrometry—Non-denaturing mass spectrometry was carried out on an LTQ Orbitrap Velos mass spectrometer equipped with electrospray source by direct injection of a 250 μM protein sample in 10 mM ammonium acetate, 0 mM NaCl, pH 6.0 (pH adjusted with ammonium hydroxide and acetic acid). The flow rate was set to 10 $\mu\text{l}/\text{min}$, the source voltage to 4.0 kV, the S-lens to 60 V, and the capillary temperature to 200 $^\circ\text{C}$. Denaturing conditions were produced by addition of 0.1% v/v formic acid.

NMR Data Collection and Analysis—All NMR work was carried out at 25 $^\circ\text{C}$ in 50 mM sodium phosphate buffer, 150 mM NaCl, 1 mM DTT, 0.02% sodium azide, pH 6.0. $\text{Cd}^{2+}/\text{Zn}^{2+}$ exchange rates were measured by adding ^{113}Cd -EDTA to a final concentration of 4 mM to a protein sample of ~ 1 mM and recording a series of ^1H - ^{15}N HSQC³ spectra over a 2-week period. A 40 mM stock solution of ^{113}Cd -EDTA was prepared by suspending 1 mg of ^{113}CdO (Cambridge Isotope Laboratories, Andover, MA) in 100 μl of a 100 mM solution of HCl, followed by addition of 100 μl of a 100 mM solution of NaOH containing 80 mM EDTA and adjusting the pH with HCl or NaOH.⁴

Unless otherwise specified, NMR data were collected on a 600 MHz UNITYINOVA spectrometer (Varian Inc, Palo Alto, CA), using a room temperature triple resonance probe. Directly detected one-dimensional ^{113}Cd spectra were recorded using a 5-mm broadband probe, and spectra were referenced relative to $^{113}\text{CdSO}_4$ by setting the chemical shift of ^{113}Cd -EDTA to 90 ppm (27). ^1H - ^{113}Cd HMQC spectra without gradient enhancement were recorded using a 5-mm broadband probe; 32 t_1 increments of 1000 transients each were recorded with a transfer delay of 12.5 ms, corresponding to an effective coupling constant of 40 Hz. The concentration series was recorded on a Bruker Avance 600 MHz spectrometer equipped with a triple resonance cryoprobe.

NMR data were processed using NMRPipe (28) and visualized using NMRView (29). $\text{H}_2\text{O}/\text{D}_2\text{O}$ and $\text{Cd}^{2+}/\text{Zn}^{2+}$ decay rates were fitted to a two-parameter exponential using MATLAB[®] (The Mathworks, Natick, MA). Chemical shift perturbations induced by changes in protein concentration [P] were fitted to the three-parameter expression as shown in Equations 1 and 2,

$$\Delta\delta = \Delta\delta_{\text{tot}} \left\{ 1 + \frac{1}{4}p^{-1} - \frac{1}{4}\sqrt{8p^{-1} + p^{-2}} \right\} - d \quad (\text{Eq. 1})$$

where

$$p \equiv \frac{[P]}{K_D} \text{ and } \Delta\delta = \sqrt{(\Delta\delta\text{H})^2 + (\Delta\delta\text{N}/6.5)^2} \quad (\text{Eq. 2})$$

from which values for $\Delta\delta_{\text{tot}}$, K_D , and d were extracted for each residue. $\Delta\delta$ represents the composite chemical shift perturbation corresponding to perturbations $\Delta\delta\text{H}$ in the ^1H and $\Delta\delta\text{N}$ in the ^{15}N dimensions, respectively, and the factor of 6.5 accounts for the relative widths of ^1H and ^{15}N chemical shift distribu-

³ The abbreviations used are: HSQC, heteronuclear single quantum coherence; PDB, Protein Data Bank; r.m.s.d., root mean square deviation; AIR, ambiguous interaction restraint.

⁴ C. Dominguez, personal communication.

Solution Structure of RING Finger-like Domain of RBBP6

tions (30). $\Delta\delta_{\text{tot}}$ is the total chemical shift change between monomer and dimer for each residue, and d corresponds to the residual chemical shift change between the lowest accessible concentration and the zero concentration limit (pure monomer). The curves in supplemental Fig. 5 have been shifted vertically by an amount d to reflect perturbations relative to zero concentration. Curve plotting and fitting were carried out using ProFit (QuantumSoft, Uetikon am See, Switzerland).

Thermal Stability—The state of folding was monitored qualitatively using a series of ^1H - ^{15}N HSQC recorded at 5 °C intervals between 25 and 85 °C. Significant loss of dispersion between 75 and 80 °C was taken as evidence of thermally induced unfolding. On return to 25 °C, the original spectrum was restored, with negligible associated precipitation of the sample.

NMR Relaxation Measurements—The oligomeric state of RBBP6(249–335) was monitored as a function of concentration using ^{15}N relaxation measurements. The ratio of transverse and longitudinal relaxation rates, R_2/R_1 , was measured using a protocol that uses an *a priori* estimate of the correlation time and measures the deviation of the true value from this estimate (31). A set of three ^1H - ^{15}N HSQC spectra was measured at each concentration, using a sequence that incorporates an R_1 relaxation delay as follows: (a) 125.4 ms, (b) 376.2 ms, or (c) R_2 relaxation delay of 25.8 ms. Peak intensities yield R_2/R_1 values according to Equation 3.⁵

$$\frac{R_2}{R_1} = \left(\frac{I_b - I_c}{I_b - I_a} \right) \cdot \frac{t_{1a}}{t_{2c}} - \left(\frac{I_a - I_c}{I_b - I_a} \right) \cdot \frac{t_{1b}}{t_{2c}} \quad (\text{Eq. 3})$$

To assess the oligomeric state of wild type and mutant RBBP6(249–335), expected R_2/R_1 values for monomeric and dimeric proteins were estimated using an empirical relationship between the number of amino acids and the correlation time for overall rotation described by Daragan and Mayo (32). These values were then used to determine ^{15}N R_1 and R_2 relaxation delays that should yield identical peak intensities if the true R_2/R_1 value matches the expected value. One-dimensional ^{15}N -edited ^1H spectra were recorded with an R_2 relaxation delay of 51.56 ms and R_1 relaxation delays of 200.9 ms (monomer) and 723.2 ms (dimer) and compared.

Structure Determination—Assignment of backbone and side-chain resonances was carried out using standard triple resonance procedures (33). NOEs were collected from homonuclear NOESY, ^{15}N -edited NOESY, and ^{13}C -edited NOESY spectra centered on the aliphatic and aromatic regions of the ^{13}C spectrum, respectively. Restraints on backbone torsion angles were generated from backbone resonance assignments using the TALOS algorithm (34). H^{N} exchange times were measured by resuspending a sample previously lyophilized out of H_2O in D_2O and recording a series of ^1H - ^{15}N HSQC spectra over the course of 2 days. Peaks intensities plotted as a function of time were fitted to a two-parameter exponential decay function using ProFit (QuantumSoft, Uetikon am See, Switzerland).

Simulated annealing with automated assignment of NOE-derived restraints was carried out using CYANA (35, 36). Zinc

coordination was imposed by restraining the distance between the zinc ion and the sulfur atom of each cysteine residue to between 2.15 and 2.45 Å. Tetrahedral geometry was imposed by restraining the distance between each pair of sulfur atoms to between 3.55 and 3.95 Å and the distances between the zinc ion and the H^{β} protons of the coordinating cysteine to between 3.0 and 3.6 Å (37). Hydrogen bond restraints were added if the corresponding H^{N} resonance exhibited a measurable $\text{H}_2\text{O}/\text{D}_2\text{O}$ exchange time with <20% fitted error, and if the bond was present in 90% of unrestrained structures.

Docking of monomers was carried out in HADDOCK using the standard parameter set augmented with C_2 symmetry, with the imposition of inter-molecular ambiguous interaction restraints (AIRs) but no NMR-derived intra-molecular restraints. AIRs were generated by specifying residues with dimerization-induced chemical shifts greater than 0.1 ppm as “active” and the complete interface as “passive.” Following calculation of the structure of the homodimer using the CANDID protocol in CYANA, the structures were returned to HADDOCK and recalculated as done previously, but this time with imposition of all unambiguous NOE-derived restraints from the CANDID runs and AIRs as described above. 400 HADDOCK structures were generated of which 32 structures were selected on the basis of low HADDOCK energy, low NOE violations (<0.5 Å), and validation scores from WHATCHECK (38) and PROCHECK NMR (39).

Protein-Protein Interactions—The yeast two-hybrid screen was carried out as described previously (15) using a cDNA bait corresponding to residues 1–81 of human RBBP6. His₆-tagged proteins IntC and toxin A were used as dummy interactors in the His₆ pulldown assay, and GST-tagged peroxiredoxin Prx2 from *Xerophyta viscosa* was used in the GST pulldown assay. Assembly of the pGFP-RBBP6 construct was described previously (15).

RESULTS

Sequence Analysis—An alignment of the RING finger-like sequences from orthologues of human RBBP6 is shown in supplemental Fig. 1, along with a number of other U-box and RING finger domains. In the overwhelming majority of eukaryotic genomes, the domain forms part of a single copy gene alongside an N-terminal DWNN domain and a CCHC zinc knuckle domain (see Fig. 1A). However a distantly related form of the protein found in the primitive single-celled eukaryotes *Tetrahymena thermophila* (XP_001020977) and *Paramecium tetraurelia* (XP_001434055) contains the DWNN domain fused directly to the RING finger domain, followed by a YT521-B homology (YTH) domain, which, interestingly, is also found in splicing factors (40). YTH domains bind single-stranded mRNA (41), and it is therefore possible that they play the same role as the CCHC zinc knuckle in these proteins. A number of fungal genomes contain a closely related copy of the domain at the N terminus of an otherwise apparently unrelated protein. The primitive eukaryote *Giardia lamblia* is the only fully sequenced eukaryotic genome in which we were unable to identify an RBBP6-like protein.

The pattern of eight cysteine residues is highly conserved across the RBBP6 family, suggesting that the domain binds two

⁵ Bruno Kieffer, personal communication.

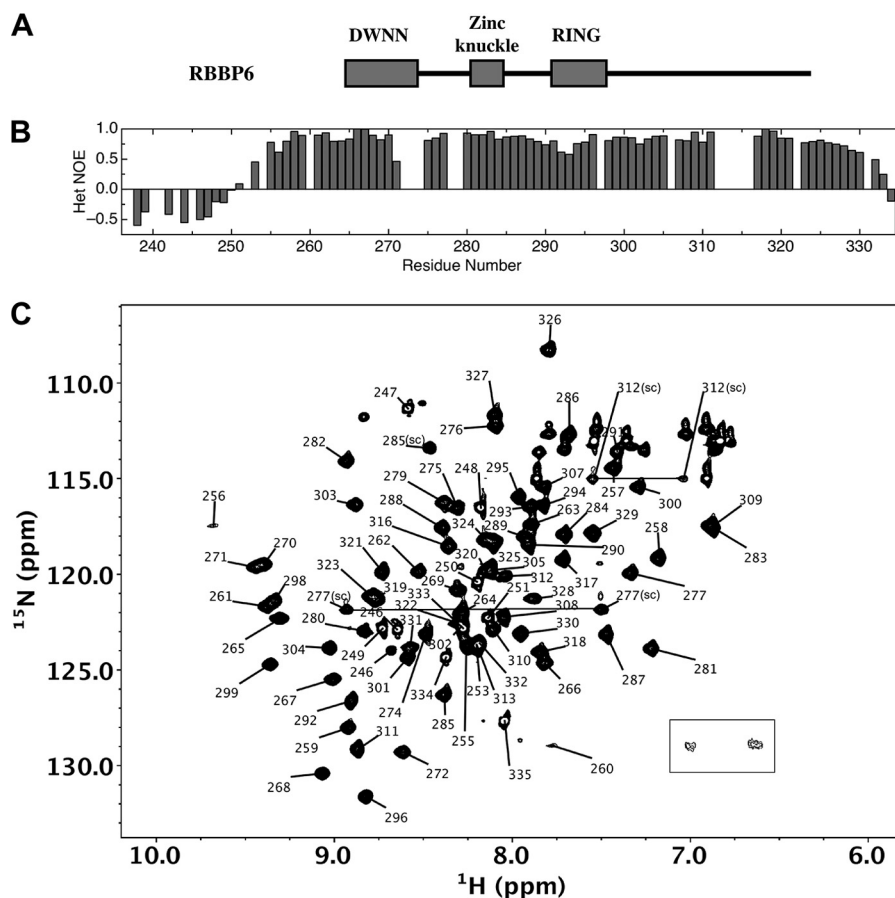


FIGURE 1. *A*, domain structure of the minimal RBBP6 transcript expressed in all eukaryotes. *B*, heteronuclear NOE of residues 236–335 of RBBP6 as a function of residue number. The structured region corresponds to residues 250–333. *C*, ^1H - ^{15}N HSQC spectrum of RBBP6(249–335). The side-chain NH_2 resonances of Asn²⁷⁷, which have highly unusual chemical shifts, and of Asn³¹², which are severely broadened, are indicated by horizontal lines and label *sc*. The presence of the side-chain NH_2 resonances of Arg²⁸⁵ (boxed) indicates that they are buried and most probably involved in salt-bridge interactions. (These resonances are plotted at a lower level from the rest of the spectrum to reduce noise. They are aliased from the true nitrogen chemical shift of 72.1 ppm.)

zinc ions in common with RING fingers. The second pair of cysteine residues forms a highly characteristic “CC” motif that is almost completely conserved across the RBBP6 family and differs from the CX_{1-2}H found at this position in C3HC4 RING fingers or the CX_{1-2}C found in C4C4 RING fingers. The only exceptions we were able to find were the primitive single-celled eukaryotes *Encephalitozoon cuniculi* and *Enterocytozoon bieneusi*, in which the C4C4 motif reverts to the canonical C3HC4 motif. In a number of fungi, including yeasts *Saccharomyces cerevisiae* and *Pichia pastoris*, the first and third pair of cysteine residues, which together coordinate the same zinc ion, have been lost, suggesting that these proteins bind only one zinc ion, with the other ion possibly being replaced by a hydrogen bond network similar to that found in U-boxes. In other fungi, such as the fungus *Aspergillus niger*, the second cysteine has been replaced by aspartic acid.

In RBBP6 sequences from higher eukaryotes an asparagine residue is found at the position occupied by histidine in C3HC4 RING fingers (see supplemental Fig. 1), raising the question as to whether it is involved in zinc coordination (42). Surveys of metal-binding proteins in the Protein Data Bank suggest that direct coordination of zinc ions by asparagine residues (so-called “first shell” ligands) is highly unlikely (43); however, they are found to stabilize zinc-binding sites by forming hydrogen

bonds with the sulfur atoms of coordinating cysteine residues, so-called “second shell” ligands.

Bacterial Expression and NMR Resonance Assignment—A peptide corresponding to residues 236–335 of human RBBP6 was expressed in *Escherichia coli*, and sequence-specific assignment was performed according to standard triple resonance NMR procedures (33). A ^1H - ^{15}N heteronuclear NOE spectrum (44) showed that residues 251–333 constitute a rigid domain, with residues 236–248 forming a flexible N-terminal extension (Fig. 1*B*). A shorter peptide corresponding to residues 249–335 was therefore expressed and used for all subsequent analyses. With the exception of the excluded residues, the ^1H - ^{15}N HSQC spectrum of the new fragment was essentially the same as that of the previous fragment (data not shown); however the ^1H - ^{15}N HSQC spectrum of a shorter fragment beginning at residue 255 revealed it to be unfolded (data not shown), leading us to conclude that residues 249–335 constitute the minimal independently folding domain. The domain was found to be highly stable in solution, with a number of samples remaining stable for more than a year at 4 °C with minimal deterioration of the ^1H - ^{15}N HSQC spectrum. Preliminary NMR data suggest that the domain has high thermal stability, with at least some elements of structure surviving up to 75 °C, as shown in supplemental Fig. 2.

Solution Structure of RING Finger-like Domain of RBBP6

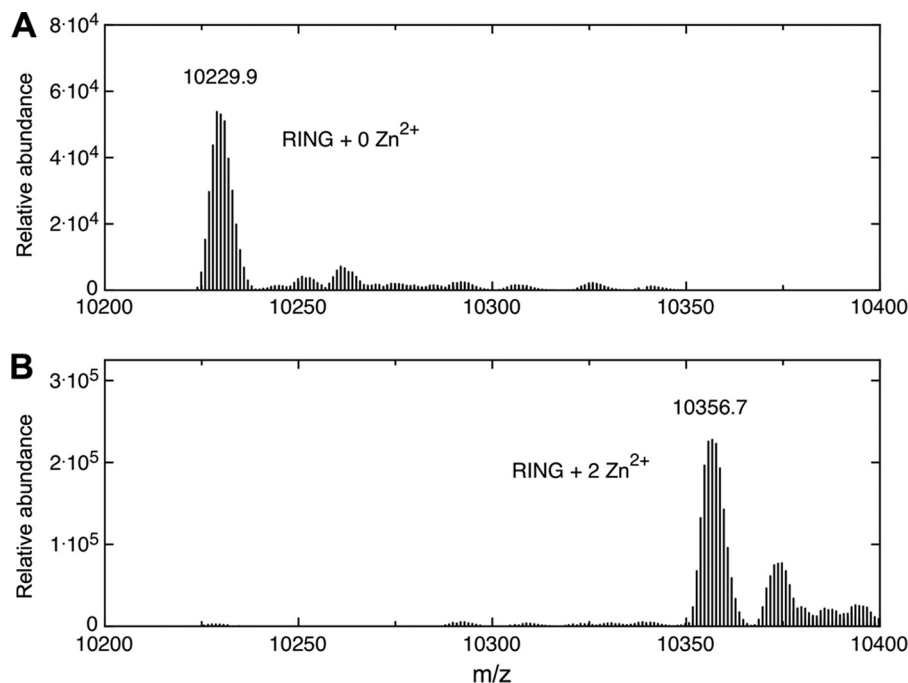


FIGURE 2. **Electrospray mass spectrograms of RBBP6(249–335) in nondenatured (native) and denatured conditions.** The mass difference of 127 Da is consistent with the binding of two Zn^{2+} ions by the native state, which are not present in the denatured state.

^{15}N , ^{13}C -Enriched samples of the domain were prepared, and chemical shift assignments were obtained for all backbone resonances with the exception of Phe³¹⁴ and Leu³¹⁵ and for all nonexchanging side-chain resonances. Of interest are the highly unusual shifts of the side-chain NH_2 group of Asn²⁷⁷ (Fig. 1C) as follows: $\delta\text{H}^{\delta 21} = 8.90$, $\delta\text{H}^{\delta 22} = 7.50$, and $\delta\text{N}^{\delta 2} = 122.4$ ppm, compared with expected shifts of 7.35 ± 0.48 , 7.13 ± 0.48 , and 112.77 ± 2.24 ppm, respectively (Biological Magnetic Resonance Data Bank). The H^α resonance of neighboring Ser²⁷⁸ is shifted downfield to 6.07, compared with an expected shift of 4.50 ± 0.43 ppm, and the H^β resonances are shifted upfield to 3.00 and 3.40 from 3.85 ± 0.30 ppm, respectively. The H^N resonances of Glu²⁵⁶ and Leu²⁶⁰ and the side-chain NH_2 resonances of Asn³¹² are highly broadened. The H^γ hydroxyl resonance of Tyr²⁷⁹, which is usually not observed due to exchange with the solvent, appears at the unusual shift of 6.0 ppm (compared with an expected shift of 9.13 ± 2.70 ppm), suggesting that it is protected from the solvent by hydrogen bonding. Similarly, the $\text{H}^{\eta 1}$ and $\text{H}^{\eta 2}$ resonances of Arg²⁸⁵, which are usually not observed due to exchange with the solvent, appear as broadened peaks in the ^1H - ^{15}N HSQC spectrum at $(\delta\text{H}, \delta\text{N}) = (7.0, 72.1)$ and $(6.7, 72.1)$ ppm, respectively (boxed in Fig. 1C), suggesting that they are also involved in hydrogen bonding or salt bridges.

Metal Binding—Electrospray ionization mass spectrometry revealed a mass difference of 127 Da between the native and the denatured states of the protein (Fig. 2), which is consistent with binding of two Zn^{2+} ions (M_r , 65.4 each) by the native state.

In the presence of EDTA, the protein did not immediately unfold but precipitated slowly over the course of 1–2 weeks, suggesting that the zinc ions are very tightly bound. The protein remained unfolded even after removal of the EDTA, as determined from its ^1H - ^{15}N HSQC spectrum, but it folded immedi-

ately on addition of 2 mM ZnSO_4 , yielding a spectrum indistinguishable from the original (data not shown). Investigation of the pH dependence of folding by monitoring the one-dimensional proton NMR spectrum revealed that the protein unfolded almost completely when the pH was reduced from 6.0 to 5.5 (data not shown), which is consistent with protonation of the cysteine thiolate groups and corresponding loss of Zn^{2+} ions at lower pH (45, 46).

Following addition of 2 mM CdCl_2 , the ^1H - ^{15}N HSQC spectrum of the zinc-bound form was replaced by a cadmium-bound form over the course of a 2-week period (Fig. 3A). The stability of the cadmium-bound form appeared to be comparable with that of the zinc-bound form, surviving for a number of weeks in cadmium-free buffer. Following dialysis into a buffer containing 2 mM ZnCl_2 , the ^1H - ^{15}N HSQC spectrum returned to its original zinc-bound form over approximately the same time period, indicating that the exchange was fully reversible.

The ^1H - ^{15}N HSQC spectrum of the cadmium-bound form was assigned by comparing ^{15}N -edited NOESY spectra recorded on each form, although in the majority of cases the shifts were sufficiently small to make this unnecessary. The magnitudes of the ^1H and ^{15}N chemical shift changes are shown as a function of residue number in Fig. 3B. Peak intensities were extracted as a function of time (supplemental Fig. 3) and used to determine the metal ion exchange rate for each residue. Two different rates are readily discernible in Fig. 3C, corresponding to binding Sites 1 ($0.22 \pm 0.06 \text{ day}^{-1}$) and 2 ($0.35 \pm 0.10 \text{ day}^{-1}$), respectively. These rates are approximately an order of magnitude slower than those obtained for other C4C4 RING domains (see Table 1), despite the fact that the measurements were made at pH 6 (as compared with pH 7 for the other two proteins in Table 1), where the rates might be expected to be faster in view of the fact that the protein starts to unfold just below pH 6.

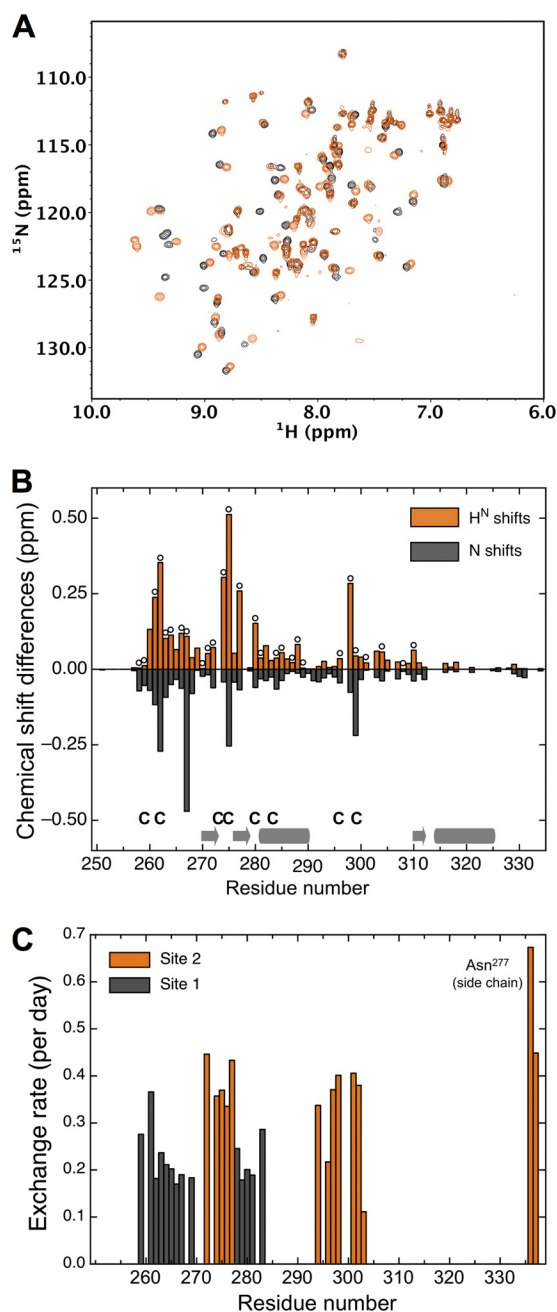


FIGURE 3. *A*, overlay of ^1H - ^{15}N HSQC spectra of Cd^{2+} -bound (*sepia*) and Zn^{2+} -bound (*gray*) samples, showing chemical shift differences. *B*, ^1H and ^{15}N chemical shift changes resulting from exchange of cadmium for zinc. Nitrogen chemical shift changes are scaled as described under “Experimental Procedures” to represent the true biological significance. Circles above the bars indicate slowly exchanging backbone amides. *C*, rates of decay of the zinc-bound form as a function of residue number. Two rates are broadly discernible, correlating with residues close to Site 1 (*gray*; slowly exchanging) or Site 2 (*sepia*; rapidly exchanging). On the basis of their rapid exchange, the side-chain NH_2 resonances of Asn^{277} can be assigned to Site 2.

$\text{Cd}^{2+}/\text{Zn}^{2+}$ exchange was monitored directly using a directly detected one-dimensional ^{113}Cd NMR spectrum. The peak at 90 ppm (see Fig. 4A) corresponds to ^{113}Cd -EDTA, and those at 729 and 711 ppm to $^{113}\text{Cd}^{2+}$ ions bound into the two sites of the protein, respectively. ^{113}Cd chemical shifts in the range 700 to 750 ppm correspond to tetrahedral coordination, with octahedral coordination in the vicinity of -110 ppm (47), from which we conclude that the Cd^{2+} ions are tetrahedrally coordinated in

TABLE 1

Zinc/cadmium exchange rates for RING finger domains from three different proteins

Domain	Exchange rate		^{113}Cd chemical shift	
	Site 1	Site 2	Site 1	Site 2
CNOT4 ^a	7.4 ± 0.7	3.4 ± 0.2	688	714
p44 ^b	18.2 ± 1.1	29.8 ± 1.7	695	676
RBBP6 ^c	0.22 ± 0.06	0.35 ± 0.10	711	729

^a Exchange rates are from Houben *et al.* (57); chemical shifts are from Hanzawa *et al.* (37).

^b Exchange rates are from Houben *et al.* (57); chemical shifts are from Kellenberger *et al.* (12).

^c Data are from this work.

both sites. During the $\text{Zn}^{2+}/\text{Cd}^{2+}$ exchange experiment, the amplitudes of the ^{113}Cd -EDTA peak decreased, and the two protein-bound peaks increased at a rate qualitatively consistent with those measured using ^1H - ^{15}N HSQC spectra (data not shown), with the slower exchange rate corresponding to the resonance at 711 ppm. We conclude that the resonance at 711 ppm corresponds to the ion coordinated by the first and third pairs of cysteine residues (Site 1) and 729 ppm to the ion coordinated by the second and fourth pairs (Site 2).

To confirm the identities of the residues coordinating each ion, a ^1H - ^{113}Cd HMQC spectrum was recorded with the aim of observing correlations between the H^β nuclei belonging to the coordinating cysteine residues and the bound $^{113}\text{Cd}^{2+}$ ions. Fig. 4B shows that there is coherence transfer between the two cadmium nuclei and a number of ^1H nuclei with resonances around 3 ppm, which is characteristic of the H^β nuclei of cysteine residues. Closer analysis allowed assignment of Cys^{262} , Cys^{280} , and Cys^{283} in Site 1 and Cys^{274} , Cys^{275} , and Cys^{299} in Site 2. Although Cys^{259} and Cys^{296} were not observed in the ^1H - ^{113}Cd HMQC spectrum, they were assumed to be involved in coordination due to their conservation and the fact that the ^{113}Cd chemical shifts are both consistent with tetrahedral coordination. Furthermore, because both cysteine residues in the “CC” motif (Cys^{274} and Cys^{275}) were directly observed in the ^1H - ^{113}Cd HMQC, we conclude that RBBP6(249–335) is indeed a C4C4 RING finger domain.

Homodimerization—To investigate whether the RBBP6 RING finger-like domain homodimerizes *in vitro*, we performed a concentration series to observe the effect of concentration on backbone chemical shifts and relaxation properties. Fig. 5 shows a superposition of ^1H - ^{15}N HSQC spectra recorded at concentrations ranging from 1000 to 25 μM . There is a marked concentration-dependent shift in a number of residues and little or no change in the rest, consistent with a change in the oligomeric state of the molecule rather than an overall conformation change. ^{15}N relaxation measurements, which provide an estimate of the correlation time for isotropic tumbling in solution (48), confirmed that at the lowest concentrations the molecule is almost completely monomeric, although at higher concentrations it is almost completely dimeric (supplemental Fig. 4).

Chemical shift changes were plotted as a function of concentration (supplemental Fig. 5) and fitted to a homodimeric binding curve (Equation 1 under “Experimental Procedures”), from which the effective K_D value of dimerization was extracted for

Solution Structure of RING Finger-like Domain of RBBP6

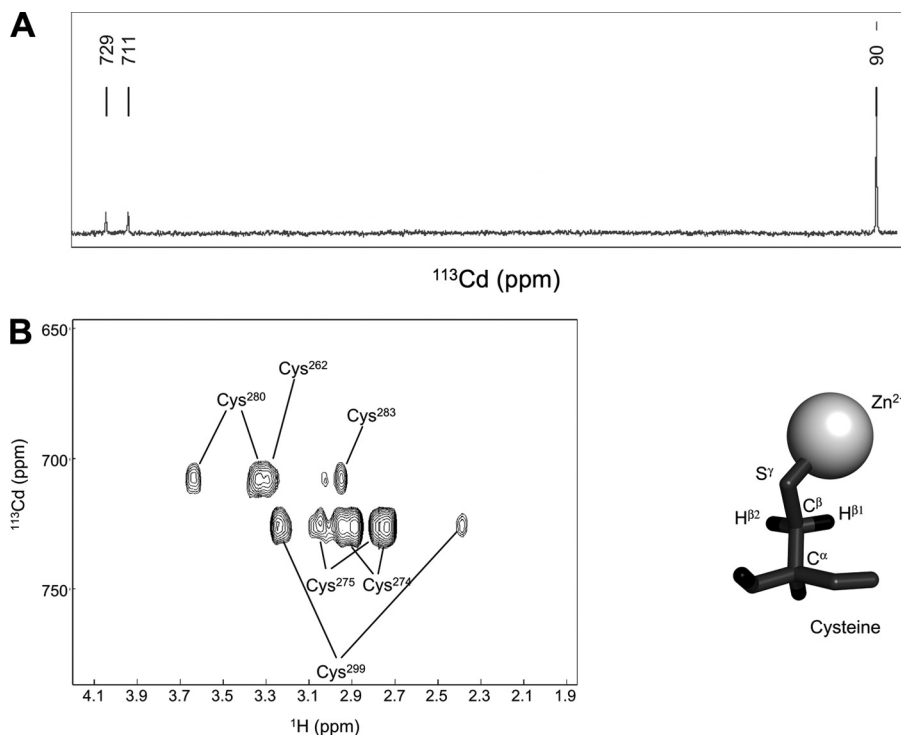


FIGURE 4. *A*, directly detected ^{113}Cd spectrum of the RBBP6(249–335) a number of days following addition of ^{113}Cd -EDTA. The single peak at 90 ppm corresponds to ^{113}Cd bound to EDTA and the peaks at 711 and 729 ppm correspond to ^{113}Cd bound into Sites 1 and 2 respectively. *B*, ^{113}Cd - ^1H -HMOC spectrum of ^{113}Cd -exchanged domain. Cross-peaks arise from three-bond couplings between the Zn^{2+} ion and the H^β protons of cysteine residues (shown at right). Six of the eight cysteines (Cys²⁶², Cys²⁸⁰, and Cys²⁸³ in Site 1 and Cys²⁷⁴, Cys²⁷⁵, and Cys²⁹⁹) could be assigned.

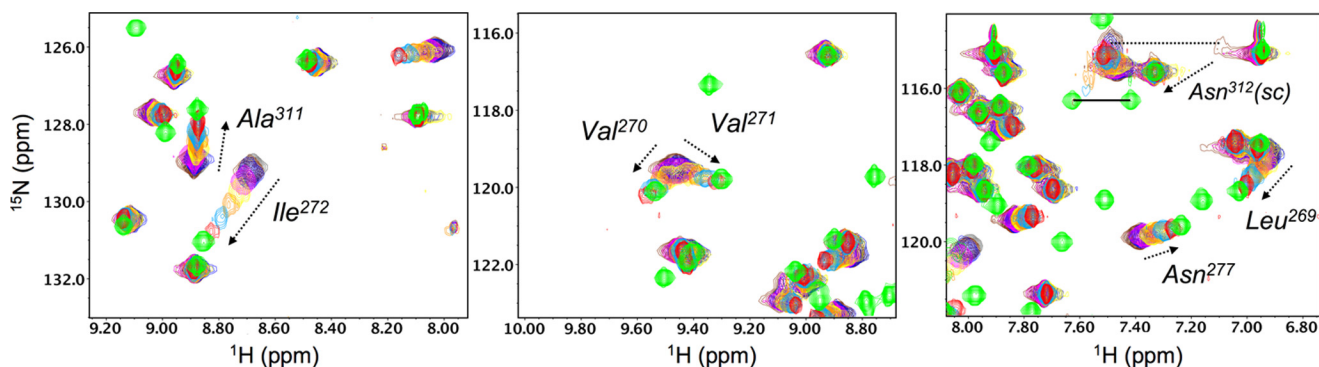


FIGURE 5. **Overlay of ^1H - ^{15}N HSQC spectra of the wild type RBBP6(249–335) at a range of different concentrations from 1000 μM , at which it is approximately dimeric, to 25 μM , at which it is approximately monomeric.** Arrows point in the direction of decreasing concentration. In many cases the spectrum of the K313E mutant (in green) corresponds to the low concentration limit of the wild type spectra, indicating that K313E is monomeric. The horizontal lines in the right-hand panel join the side-chain NH_2 resonances of Asn³¹², which are severely broadened in the wild type (dotted line; highest concentration) but much narrower in the mutant (solid line). As with the backbone amides, the position of the side-chain NH_2 of Asn³¹² in the mutant corresponds to the low concentration limit of the wild type spectra, indicating that K313E is monomeric.

each residue. The values of K_D and the total chemical shift change ($\Delta\delta_{\text{tot}}$) for residues shifting by more than 0.1 ppm (composite chemical shift) are presented in supplemental Table 1. The average K_D is of the order of $100 \pm 30 \mu\text{M}$.

Solution Structure—Because chemical shift perturbations suggested that dimerization did not significantly alter the structure of the monomer, monomeric structures were first calculated using CYANA and then “soft-docked” using HADDOCK (49) with the aid of AIRs generated from the chemical shift perturbations. On the basis of the docked homodimers, a number of unambiguous inter-molecular NOEs were identified that were used to guide a full CYANA calculation of the homodimer structure. Finally, the structures were returned to HADDOCK and subjected to refine-

ment in explicit solvent (not available in CYANA) using the complete set of unambiguous restraints generated by CYANA, including 146 intermolecular NOE-derived restraints.

Superposition of the 32 best structures yielded average r.m.s.d. values of $0.89 \pm 0.23 \text{ \AA}$ for backbone heavy atoms and $1.21 \pm 0.25 \text{ \AA}$ for all heavy atoms in structured regions. A summary of restraints and structural statistics is presented in Table 2. A superposition of the backbone traces and a representative schematic are shown in Fig. 6, *A* and *B*, respectively.

Analysis of a representative structure by the PISA server revealed that the homodimer buries 787.9 \AA^2 of surface area with a free energy change of $\Delta G_i = -8.3 \text{ kcal}\cdot\text{mol}^{-1}$. The p value of 0.18 indicates that the homodimer most probably

results from a specific interaction ($p > 0.5$ corresponds to a random or nonspecific interaction).

The secondary structure includes the β - β - α - β motif typical of RING finger domains, with three short β -strands forming a

TABLE 2

Structural statistics for the RING finger-like domain from human RBBP6

Restrains (per monomer)	
NOE-derived	
Intra-residue	512
Sequential	650
Medium	526
Long	826
Intra-molecular	146
Dihedral angle (TALOS)	92
Hydrogen bonds	
bb-bb	22 (intra) + 1 (inter)
sc-sc/bb	5 (intra) + 3 (inter)
NH-S	2 (intra)
Restraint violations	
NOE violations >0.2 Å	7.5 ± 2.7
NOE violations >0.3 Å	1.4 ± 0.8
Dihedral violations $>5^\circ$	0.0 ± 0.0
Zn²⁺ coordination geometry	
S ^{γ} -Zn ²⁺ distance	2.30 ± 0.15 Å
S ^{γ} -S ^{γ} distance	3.75 ± 0.20 Å
C ^{β} -Zn ²⁺ distance	3.30 ± 0.30 Å
S ^{γ} -Zn ²⁺ -S ^{γ} coordination angles	$109.5 \pm 6.6^\circ$
Pairwise r.m.s.d. (Å) ^a	
Backbone heavy atoms	0.89 ± 0.23
All heavy atoms	1.21 ± 0.25
Residues in regions of Ramachandran plot (%)	
Most favored	85.6 ± 1.0
Additionally allowed regions	13.3 ± 1.1
Generously allowed regions	1.2 ± 0.4
Disallowed regions	0.0 ± 0.0

^a Fitting was performed over residues 256–329 of both monomers. All parameters were calculated over structured regions, residues 249–329.

triple-stranded anti-parallel sheet (β_1 , residues 270–272; β_2 , residues 276–279; α_1 , residues 281–290; and β_3 , residues 310–311). The core is made up of the side chains of Val²⁷⁰, Ile²⁷², Tyr²⁷⁹, Ile²⁸⁴, Leu²⁸⁸, Val³⁰⁴, and Leu³⁰⁹, which correspond to conserved hydrophobic residues in most RING domains and U-boxes (see supplemental Fig. 1). In addition, the domain contains the C-terminal helix (α_2 , residues 314–325) found in many U-boxes, which packs against a structured N-terminal loop (residues 252–257). This creates a second core region made up of the hydrophobic side chains of Ile²⁵³, Pro²⁵⁴, Leu²⁵⁷, and Ile²⁶⁵, contributed by the N-terminal strand, and Val³¹⁹ and Phe³²², contributed by the C-terminal helix, all of which are conserved in RING and U-box domains featuring the C-terminal helix. The packing of Ile²⁵³ and Pro²⁵⁴ against the side chain of Phe³²² accounts for the fact that deletion of these residues in RBBP6(255–335) resulted in an unfolded protein.

The structure contains a large number of protected amides, represented by *open circles* in Fig. 3B. Although some of these can be explained on the basis of hydrogen bonding in secondary structural regions (shown in schematic form at the *bottom* of Fig. 3B), others such as Leu²⁶¹, Cys²⁶², Cys²⁶⁴, Cys²⁷⁵, Asn²⁷⁷, Cys²⁸⁰, and Thr²⁹⁸ cannot be accounted for in this manner. Furthermore, as can be seen from Fig. 3B, these correspond to the residues with the largest ¹H chemical shift changes on cadmium binding. Analysis of the structures suggests that these correspond to hydrogen bonds between backbone/side-chain amides and the S ^{γ} atoms of cysteine residues involved in zinc coordination. A corresponding pattern of hydrogen bonds between backbone amides and residues taking the places of the cysteine residues is found in U-boxes, where they provide the

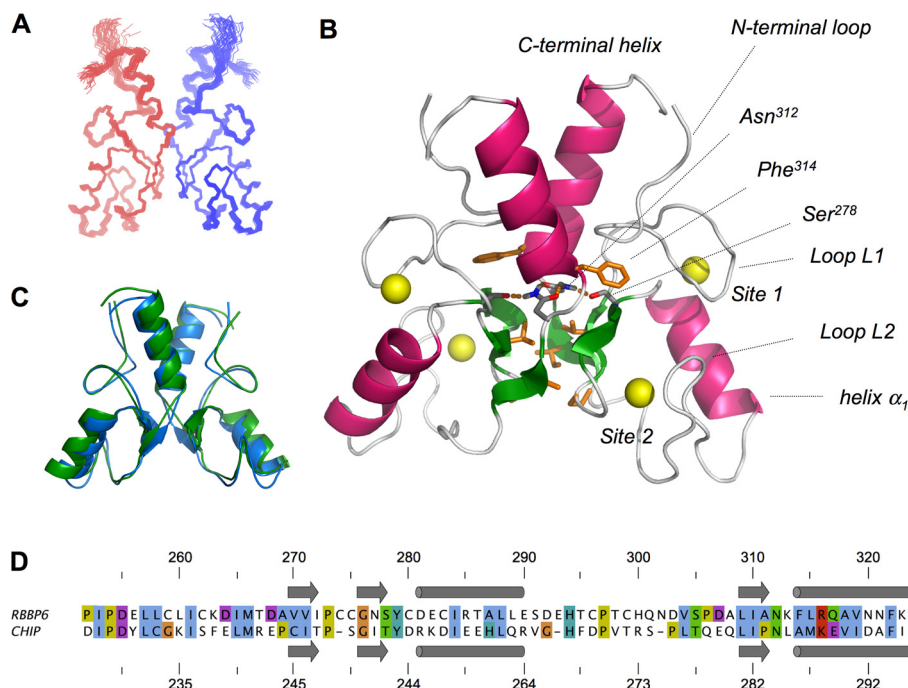


FIGURE 6. *A*, overlay of backbone traces for the family of 32 lowest energy structures of the homodimer. *B*, schematic showing the secondary structure of the homodimer, with interface consisting of the triple-stranded β -sheets (green) and the C-terminal helices (pink). Zinc ions are shown as yellow spheres. The interface contains a significant number of hydrophobic residues (brown), including Phe³¹⁴, which projects deep into the opposing monomer. At the center of the interface, Asn³¹² makes a pair of reciprocal hydrogen bonds with its counterpart in the opposing monomer. *C*, overlay of the backbone schematic of RBBP6(249–335) (blue; this work) and the U-box domain from murine CHIP (green, PDB code 2C2L) and corresponding structural alignment (*D*). Secondary structural elements are indicated in gray.

Solution Structure of RING Finger-like Domain of RBBP6

stabilization required to make up for the lack of zinc coordination. Our data therefore suggest that the domain is stabilized by a similar network of hydrogen bonds to that found in U-boxes, in addition to the stabilization provided by zinc binding. To our knowledge, this has not been previously reported in other RING finger domains.

A search of the Protein Data bank by the Dali server (50) using the structure of the monomer (residues 252–326) found that the structure most closely resembles a number of U-boxes, including those from murine CHIP (PDB code 2C2L, *Z*-score 11.1, r.m.s.d. 1.6 Å) and yeast Ufd2p (PDB code 3M62, *Z*-score 10.9, r.m.s.d. 1.8 Å). The highest ranking RING finger proteins were TRIM37 (PDB code 3LRQ, *Z*-score 10.4, r.m.s.d. 2.1 Å) and the Polycomb Group RING finger proteins RING1b and Bmi1 (PDB code 2CKL, *Z*-score 10.1, r.m.s.d. 1.9 Å), all of which have been described as U-box-like (51). CHIP and TRIM37 form homodimers and RING1b and Bmi1 a heterodimer, whereas Ufd2p is monomeric. Superposition of the full homodimer on the U-boxes from CHIP, TRIM37, and RING1b/Bmi gives *Z*-scores of 19.9, 16.7, and 16.1, respectively.

An overlay of the backbone schematics of RBBP6 and CHIP is shown in Fig. 6C and the corresponding structural alignment in Fig. 6D. Equivalent residues in the interface are listed in supplemental Table 2. The largest part of the interface is formed by the two β -sheets, which come together to create a pseudo six-stranded β -barrel burying hydrophobic residues Val²⁷¹, Pro²⁷³, Gly²⁷⁶, and Ile³¹⁰ from each monomer. Phe³¹⁴ docks into a deep pocket in the opposite monomer formed by Leu²⁵⁷, Leu²⁶⁰, Met²⁶⁶, and Leu³¹⁵, a conclusion supported by the presence of a number of inter-molecular NOEs and the broadening of the backbone resonances of Phe³¹⁴.

In a number of U-boxes a pivotal role is played by an asparagine (e.g. Asn²⁸⁴ in murine CHIP) positioned close to the 2-fold axis, which forms a reciprocal pair of hydrogen bonds with its counterpart in the opposite monomer (52). Asn³¹² occupies the equivalent position in this case; large dimerization-induced perturbations of the chemical shifts of the backbone H^N and side-chain H ^{δ 2} resonances (supplemental Table 1) suggest that it makes similar reciprocal hydrogen bonds as found in the U-boxes. The structures also provide evidence for a hydrogen bond between Ser²⁷⁸ and Asn³¹², which is supported by broadening of all resonances belonging to Ser²⁷⁸. The equivalent interaction is observed in crystal structures of CHIP (PDB codes 2F42 and 2C2L, although Ser²⁷⁸ is substituted by a threonine residue), where it is described by Xu *et al.* (53) as “orienting” the asparagine for its reciprocal interaction across the interface. In the hydrophobic context of the rest of the interface, this network of polar interactions is likely to exercise a strong stabilizing effect on the homodimer. Mutation of Asn³¹² to aspartic acid (N312D) abolished the homodimer completely, yielding a ¹H-¹⁵N HSQC spectrum closely approximating the low concentration limit of the concentration series (data not shown).

Severe broadening of all resonances of Lys³¹³ suggested that it may participate in a stable intermolecular salt bridge with the acidic patch formed by Asp²⁵⁵ and Glu²⁵⁶ on the opposite monomer. Mutation of Lys³¹³ to glutamic acid (K313E) also completely abolished the homodimer, yielding a ¹H-¹⁵N HSQC

spectrum closely approximating the low concentration limit of the concentration series (shown in green in the overlay in Fig. 5). The monomeric nature of both N312D and K313E mutants was confirmed using ¹⁵N relaxation (supplemental Fig. 4).

The H ^{η} resonance of Tyr²⁷⁹ is protected from exchange with the solvent, indicating that it is involved in a stable hydrogen bond. The structure confirms that Tyr²⁷⁹ is completely buried, extending through the core from the N-terminal end of helix α_1 into loop 2. In RING fingers this residue is almost always large and hydrophobic (see supplemental Fig. 1), but in both the RBBP6 family and the U-box family tyrosine is most common at this position. Formation of a hydrogen bond at the very end of the side chain enables Tyr²⁷⁹ to play the role of a reinforcing girder, contributing to the rigidity of the molecule. Although the identity of the hydrogen bond donor is not certain, possible candidates include the S ^{γ} atom of Cys²⁹⁶ and the N ^{δ 2} side-chain atom of Asn²⁷⁷. In crystal structures of CHIP, the H ^{η} atom of the corresponding tyrosine residue forms a hydrogen bond with the residue corresponding to Cys²⁹⁶ (Tyr²⁵³ H ^{η} –Asn²⁶⁹ O ^{δ 1} in mouse, PDB code 2C2L; Tyr²³³ H ^{η} –Asp²⁴⁹ O ^{δ 2} in zebrafish, PDB 2OXQ), suggesting that Cys²⁹⁶ may indeed be the acceptor in this case.

The structures suggest that the side-chain NH₂ group of Asn²⁷⁷ forms a hydrogen bond with the S ^{γ} atom of Cys²⁷⁵ in Site 2, providing a possible explanation for its highly unusual chemical shifts. The chemical shift perturbations on cadmium exchange (>0.1 ppm for both H ^{δ 2} protons) suggest a stable association with the coordination center. Interestingly, the orthologous domain from *S. cerevisiae* (see supplemental Fig. 1) contains an asparagine in a similar position showing virtually identical chemical shifts,⁶ which suggests that the effect may be a feature of side-chain NH₂ groups involved in NH–S hydrogen bonds. Ongoing structural analysis of other members of the RBBP6 family may shed more light on this.

Analysis of the structures indicates a possible long range salt bridge between Asp²⁶⁸ and Arg³¹⁶, which is also present in PUB14 (54), where arginine is replaced by lysine (Asp²⁶³–Lys³⁰⁸), and possibly also in CHIP. This interaction would account for the high level of conservation at both of these positions in the RBBP6 and U-box families. We see no evidence for the salt bridges corresponding to Lys²⁶²–Glu²⁷¹ and Lys²⁶²–Glu³²¹ seen in PUB14 (54).

The appearance in the ¹H-¹⁵N HSQC spectrum of both side-chain NH₂ groups of Arg²⁸⁵ (see Fig. 1C) indicates that these groups are involved in stable interactions. Candidate interactions include a long range hydrogen bond with Pro³⁰⁶ O and a short range salt bridge with Asp²⁸¹, which is adjacent to Arg²⁸⁵ on helix α_1 . Both of these interactions would require Arg²⁸⁵ to lie parallel to the surface of the molecule, presumably contributing to its stability. In support of this, crystal structures of CHIP (PDB codes 2OXQ and 2C2L) show the equivalent salt bridge involving an arginine oriented parallel to the surface (Arg²⁵⁵ and Glu²⁵⁹ in murine CHIP), although the positions of the interacting residues are swapped (see supplemental Fig. 1). Following mutation of Asp²⁸¹ to alanine (D281A) the side-

⁶ F. Hassem and D. J. R. Pugh, unpublished data.

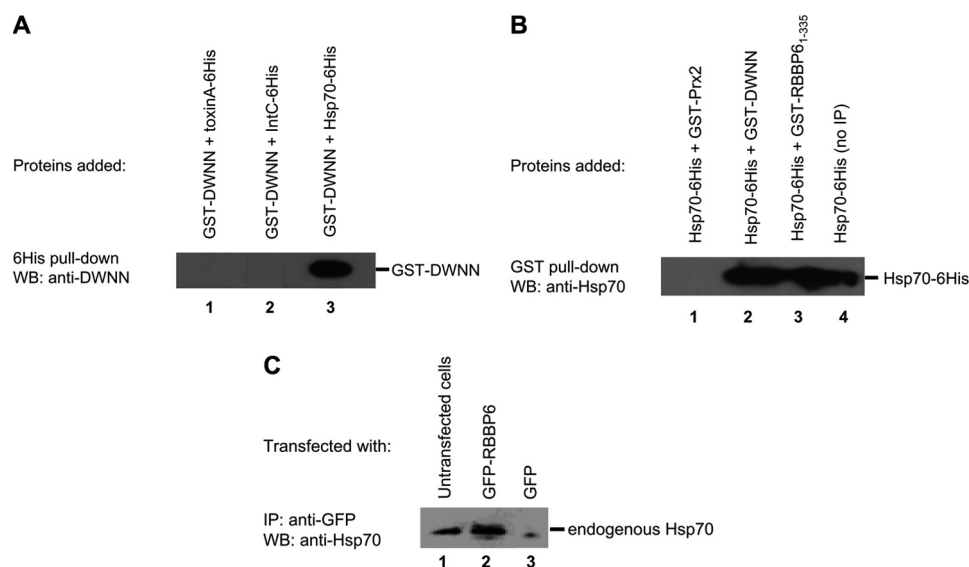


FIGURE 7. **N-terminal DWNN domain of human RBBP6 interacts with human heat shock protein 70 (Hsp70A1A) in vitro and in vivo.** *A*, in an immobilized metal affinity assay, His₆-tagged Hsp70 was able to precipitate a GST-DWNN fusion protein (lane 3), but two unrelated His₆-tagged proteins were not (lanes 1 and 2). Equal amounts of GST-DWNN were present in each lane. *WB*, Western blot. *B*, in the reciprocal GST affinity assay, GST-DWNN and a larger GST-tagged fragment of RBBP6 (RBBP6(1–335)) were able to precipitate Hsp70-His₆ (lanes 2 and 3), but an unrelated GST-fusion protein was not (lane 1). Equal amounts of Hsp70-His₆ were present in each lane. *C*, following transfection of GFP-tagged full-length RBBP6 into mammalian cells (HEK293), GFP-RBBP6 was able to precipitate endogenous Hsp70 (as detected using an antibody against Hsp70), whereas GFP alone was not.

chain NH₂ groups of Arg²⁸⁵ were no longer observable in the ¹H-¹⁵N HSQC spectrum.

Interaction with Chaperones—RBBP6 orthologues in lower eukaryotes consist only of the DWNN domain, the CCHC zinc knuckle, and the RING finger-like domain, suggesting that this may contain the core ubiquitin-ligase function of the protein. Because the zinc knuckle is likely to function as an RNA-binding domain, the DWNN domain remains as the most likely substrate-binding domain.

To identify potential substrates for ubiquitination, a yeast two-hybrid screen with the human DWNN domain as bait was used to screen a human testis expression library as described previously (15). Five potential interacting clones were identified, which encoded two copies of the last 82 residues of heat shock 70-kDa protein 14 (HSPA14), one copy of the last 72 residues of heat shock protein 40 (DNAJB1), two copies of the core splicing protein SmG (full-length), and one each of RANBP9, Gametogenin 1a, and Niemann-Pick disease type C2 (see supplemental Table 3). In the light of the similarities between RBBP6 and the U-box proteins reported above, the interactions with heat shock proteins were considered to be highly significant. The other hits will be pursued elsewhere.

HSPA14 is a close homologue of heat shock protein 70 (HSPA1A), containing the N-terminal ATPase domain and the substrate-binding domain but lacking the 10-kDa C-terminal subdomain (55, 56). Because the last 82 residues of HSPA14 fall within the substrate-binding domain of HSPA1A, which also forms part of Hsp70 (HSP1A), we surmised that it should therefore also bind to Hsp70 (HSPA1A). To confirm this, we expressed His₆-tagged Hsp70 and GST-tagged DWNN (RBBP6(1–81)) in *E. coli* and carried out His₆ affinity pulldown assays, detecting with a monoclonal antibody against DWNN (Fig. 7A). Hsp70 was able to precipitate the DWNN domain but two unrelated His₆-tagged proteins were not.

When the reciprocal assay was carried out, precipitating GST and detecting with an antibody against Hsp70 (Fig. 7B), RBBP6 fragments containing the DWNN domain were able to precipitate Hsp70, but an unrelated GST fusion protein was not.

Finally, to investigate whether the interaction is realized *in vivo* and in the context of the complete RBBP6 protein, GFP-tagged RBBP6 was transfected into mammalian cells and its ability to precipitate endogenous Hsp70 investigated. Fig. 7C shows that GFP-RBBP6 was able to precipitate endogenous Hsp70, but GFP alone was not.

DISCUSSION

The cysteine-rich region of retinoblastoma binding protein-6 (RBBP6(249–335)) has previously been characterized both as a zinc-binding RING finger and as a U-box. Our results confirm that the domain binds two zinc ions in the characteristic “cross-braced” fashion and that the Zn²⁺ ions could be replaced by Cd²⁺ ions without significantly affecting either the stability or the conformation. However, the rates of exchange were found to be more than 10-fold slower than any previous measurement, suggesting that the structure is unusually stable. The presence of scalar coupling between the cadmium ion in Site 2 and the H^β protons of both Cys²⁷⁴ and Cys²⁷⁵, combined with lack of evidence of coupling between the cadmium ion and the side-chain NH₂ group of Asn²⁷⁷, suggests that the structure should be classified as a C4C4 RING finger rather than a C3NC4 RING finger. Asn²⁷⁷ most probably fulfils the role of a second shell ligand, donating a HN–S hydrogen bond to the S^γ of Cys²⁷⁵.

The structure contains a large number of hydrogen bonds, including a number of NH–S hydrogen bonds between backbone NH groups and S^γ atoms of cysteines coordinating zinc ions. These NH–S bonds correlate well with NH groups with large chemical shift perturbations on Cd²⁺/Zn²⁺ exchange, a relationship that has been noted previously (57). Hydrogen

Solution Structure of RING Finger-like Domain of RBBP6

bonding networks of this kind are hallmarks of U-boxes, in which they compensate for the lack of zinc coordination. It therefore appears that the RBBP6 domain may have inherited both mechanisms of stabilization, resulting in its being doubly stabilized. This would account for the slow rate of metal ion exchange, the high thermal stability, and the long term stability in solution.

It may also explain the fact that zinc coordination appears to be at least partially dispensable in some organisms, including *S. cerevisiae* and *P. pastoris*, where the first zinc-binding site has been lost, and *A. niger*, where one of the coordinating cysteines has been replaced by an aspartic acid, making it likely that the corresponding zinc ion has either been lost or else is only weakly bound. The family therefore represents a structural intermediate between the RING finger family and the U-box family, containing examples intermediate between the two. It is tempting to speculate that the family also represents an evolutionary intermediate on the path from RING fingers to U-boxes, but a more detailed genomic analysis will be needed to substantiate this notion.

The solution structure closely resembles those of the U-box family, in particular the U-box from the C terminus of Hsp70 interacting protein (CHIP). The domain dimerizes along the identical interface to that found in CHIP, and many of the residues in the interface are conserved, including Asn³¹² and Ser²⁷⁸ (substituted by threonine in CHIP), which form a network of inter-molecular polar interactions in the middle of an otherwise highly hydrophobic interface. Asn³¹² is highly conserved in higher eukaryotes but is frequently replaced by aspartic acid in lower eukaryotes. In view of the fact that the N312D mutant disrupts the homodimer, it is tempting to propose asparagine at this position as an indicator of whether a particular orthologue will homodimerize. In support of this model, preliminary investigations suggest that the domain from *S. cerevisiae*, which has aspartic acid at the corresponding position (see supplemental Fig. 1), is monomeric in solution.⁷ However, two U-boxes which are known to be monomeric, yeast Ufd2p, and mammalian E4B (58), both have asparagine at this position so the presence of asparagine is not sufficient for dimerization.

The K_D value of homodimerization is found to be on the order of 100 μM , which corresponds to a weak interaction. This value is similar to those reported for U-boxes Prp19 (59) and PUB14 (54), both of which exhibited evidence of a mixed monomer/dimer at NMR concentrations. Although such a weak interaction is unlikely to be physiologically significant, the isolated domain does not represent a physiologically realistic scenario; it is possible that the complete protein homodimerizes with greater affinity. Because homodimerization has been shown to be necessary for the ubiquitination activity of CHIP (18), and for native functioning of Prp19 (59), it will be of interest to determine whether homodimerization has functional significance for RBBP6. The K313E and N312D mutants reported here, both of which abolish homodimerization, will be useful reagents in establishing this.

The E2-binding site on U-boxes and RING fingers is located in a hydrophobic groove lying between helix α_1 and loops L1 and L2, which contain the two zinc ions in the case of RING fingers. In human RBBP6, the residues surrounding the groove are Ile²⁶¹, Ala²⁸⁷, and Pro²⁹⁷, of which Ile²⁶¹ and Pro²⁹⁷ are highly conserved across the RBBP6 family and in U-boxes. In CHIP and BRCA1, mutation of the residue corresponding to Ile²⁶¹ to alanine leads to the abolition of E2 binding and consequent loss of activity, without affecting the dimerization state of the molecule (60, 61). Based on our structure, we therefore predict that mutating Ile²⁶¹ to alanine is likely to abolish ubiquitination activity.

U-boxes are currently classified primarily as “non-zinc-binding” RING fingers. From a functional point of view, U-boxes are differentiated from RING fingers by their interaction with chaperones, most notably with Hsp70, Hsp40, and Hsp90, and their involvement in protein quality control. The strong structural similarities presented here between the cysteine-rich domain of RBBP6 and U-boxes, combined with its association with chaperones Hsp70, Hsp40, and Hsp90, suggests that it should be classified as a U-box, notwithstanding the fact that it binds two zinc ions. Two similar examples have already been reported, the RING1b/Bmi1 heterodimer and the TRIM37 homodimer, both of which bind zinc ions despite being structurally more similar to U-boxes.

The structure has been deposited in the Protein Data Bank (PDB) under accession number 3ZTG. During the preparation of this work, the NMR structure of residues 249–309 of human RBBP6 was deposited in the PDB under accession number 2YUR without associated report. 2YUR is similar in many respects to the structure presented here, but the expressed fragment lacks the third strand of the triple-stranded β -sheet and the entire C-terminal helix and is therefore unlikely to be able to homodimerize. The Z-score between 2YUR and this structure is 6.8, compared with 11.1 between this structure and CHIP.

In conclusion, the strong similarities between the RING finger-like domain of RBBP6 and members of the U-box family, combined with its association with heat shock proteins, lead us to propose that RBBP6 plays a role in chaperone-mediated ubiquitination of unfolded protein substrates. Additional investigations will be needed to establish the validity of this hypothesis. In addition, the growing number of zinc-binding U-boxes suggests that new criteria, based ideally on function rather than zinc binding, are required to distinguish between U-boxes and RING fingers.

Acknowledgments—D. J. R. P. thanks Prof. Rolf Boelens and Dr. Tammo Diercks for advice and assistance with NMR data collection.

REFERENCES

1. Witte, M. M., and Scott, R. E. (1997) The proliferation potential protein-related (P2P-R) gene with domains encoding heterogeneous nuclear ribonucleoprotein association and Rb1 binding shows repressed expression during terminal differentiation. *Proc. Natl. Acad. Sci. U.S.A.* **94**, 1212–1217
2. Vo, L. T., Minet, M., Schmitter, J. M., Lacroute, F., and Wyers, F. (2001) Mpe1, a zinc knuckle protein, is an essential component of yeast cleavage and polyadenylation factor required for the cleavage and polyadenylation

⁷ F. Hassem and D. J. R. Pugh, unpublished data.

- of mRNA. *Mol. Cell. Biol.* **21**, 8346–8356
3. Shi, Y., Di Giannamartino, D. C., Taylor, D., Sarkeshik, A., Rice, W. J., Yates, J. R., 3rd, Frank, J., and Manley, J. L. (2009) Molecular architecture of the human pre-mRNA 3'-processing complex. *Mol. Cell* **33**, 365–376
 4. Scott, R. E., Giannakourou, T., Gao, S., and Peidis, P. (2003) Functional potential of P2P-R. A role in the cell cycle and cell differentiation related to its interactions with proteins that bind to matrix-associated regions of DNA? *J. Cell. Biochem.* **90**, 6–12
 5. Gao, S., and Scott, R. E. (2003) Stable overexpression of specific segments of the P2P-R protein in human MCF-7 cells promotes camptothecin-induced apoptosis. *J. Cell. Physiol.* **197**, 445–452
 6. Scott, R. E., and Gao, S. (2002) P2P-R deficiency modifies nocodazole-induced mitotic arrest and UV-induced apoptosis. *Anticancer Res.* **22**, 3837–3842
 7. Gao, S., Witte, M. M., and Scott, R. E. (2002) P2P-R protein localizes to the nucleolus of interphase cells and the periphery of chromosomes in mitotic cells that show maximum P2P-R immunoreactivity. *J. Cell. Physiol.* **191**, 145–154
 8. Gao, S., and Scott, R. E. (2002) P2P-R protein overexpression restricts mitotic progression at prometaphase and promotes mitotic apoptosis. *J. Cell. Physiol.* **193**, 199–207
 9. Yoshitake, Y., Nakatsura, T., Monji, M., Senju, S., Matsuyoshi, H., Tsukamoto, H., Hosaka, S., Komori, H., Fukuma, D., Ikuta, Y., Katagiri, T., Furukawa, Y., Ito, H., Shinohara, M., Nakamura, Y., and Nishimura, Y. (2004) Proliferation potential-related protein, an ideal esophageal cancer antigen for immunotherapy, identified using complementary DNA microarray analysis. *Clin. Cancer Res.* **10**, 6437–6448
 10. Li, L., Deng, B., Xing, G., Teng, Y., Tian, C., Cheng, X., Yin, X., Yang, J., Gao, X., Zhu, Y., Sun, Q., Zhang, L., Yang, X., and He, F. (2007) PACT is a negative regulator of p53 and essential for cell growth and embryonic development. *Proc. Natl. Acad. Sci. U.S.A.* **104**, 7951–7956
 11. Jones, C., Reifegerste, R., and Moses, K. (2006) Characterization of *Drosophila* mini-me, a gene required for cell proliferation and survival. *Genetics* **173**, 793–808
 12. Kellenberger, E., Dominguez, C., Fribourg, S., Wasielewski, E., Moras, D., Poterszman, A., Boelens, R., and Kieffer, B. (2005) Solution structure of the C-terminal domain of TFIIF p44 subunit reveals a novel type of C4C4 ring domain involved in protein-protein interactions. *J. Biol. Chem.* **280**, 20785–20792
 13. Simons, A., Melamed-Bessudo, C., Wolkowicz, R., Sperling, J., Sperling, R., Eisenbach, L., and Rotter, V. (1997) PACT. Cloning and characterization of a cellular p53-binding protein that interacts with Rb. *Oncogene* **14**, 145–155
 14. Pugh, D. J., AB, E., Faro, A., Lutya, P. T., Hoffmann, E., and Rees, D. J. (2006) DWNN, a novel ubiquitin-like domain, implicates RBBP6 in mRNA processing and ubiquitin-like pathways. *BMC Struct. Biol.* **6**, 1
 15. Chibi, M., Meyer, M., Skepu, A., Rees, D. J., Moolman-Smook, J. C., and Pugh, D. J. (2008) RBBP6 interacts with multifunctional protein YB-1 through its RING finger domain, leading to ubiquitination and proteosomal degradation of YB-1. *J. Mol. Biol.* **384**, 908–916
 16. Aravind, L., and Koonin, E. V. (2000) The U box is a modified RING finger. A common domain in ubiquitination. *Curr. Biol.* **10**, R132–R134
 17. Ohi, M. D., Vander Kooi, C. W., Rosenberg, J. A., Chazin, W. J., and Gould, K. L. (2003) Structural insights into the U-box, a domain associated with multi-ubiquitination. *Nat. Struct. Mol. Biol.* **10**, 250–255
 18. Nikolay, R., Wiederkehr, T., Rist, W., Kramer, G., Mayer, M. P., and Bukau, B. (2004) Dimerization of the human E3 ligase CHIP via a coiled-coil domain is essential for its activity. *J. Biol. Chem.* **279**, 2673–2678
 19. Hashizume, R., Fukuda, M., Maeda, I., Nishikawa, H., Oyake, D., Yabuki, Y., Ogata, H., and Ohta, T. (2001) The RING heterodimer BRCA1-BARD1 is a ubiquitin ligase inactivated by a breast cancer-derived mutation. *J. Biol. Chem.* **276**, 14537–14540
 20. Cyr, D. M., Höhfeld, J., and Patterson, C. (2002) Protein quality control. U-box-containing E3 ubiquitin ligases join the fold. *Trends Biochem. Sci.* **27**, 368–375
 21. Hatakeyama, S., Matsumoto, M., Yada, M., and Nakayama, K. I. (2004) Interaction of U-box-type ubiquitin-protein ligases (E3s) with molecular chaperones. *Genes Cells* **9**, 533–548
 22. Rosser, M. F., Washburn, E., Muchowski, P. J., Patterson, C., and Cyr, D. M. (2007) Chaperone functions of the E3 ubiquitin ligase CHIP. *J. Biol. Chem.* **282**, 22267–22277
 23. Younger, J. M., Ren, H. Y., Chen, L., Fan, C. Y., Fields, A., Patterson, C., and Cyr, D. M. (2004) A foldable CFTR Δ F508 biogenic intermediate accumulates upon inhibition of the Hsc70-CHIP E3 ubiquitin ligase. *J. Cell Biol.* **167**, 1075–1085
 24. Peng, H. M., Morishima, Y., Jenkins, G. J., Dunbar, A. Y., Lau, M., Patterson, C., Pratt, W. B., and Osawa, Y. (2004) Ubiquitylation of neuronal nitric-oxide synthase by CHIP, a chaperone-dependent E3 ligase. *J. Biol. Chem.* **279**, 52970–52977
 25. Waterhouse, A. M., Procter, J. B., Martin, D. M., Clamp, M., and Barton, G. J. (2009) Jalview Version 2. A multiple sequence alignment editor and analysis workbench. *Bioinformatics* **25**, 1189–1191
 26. Caffrey, D. R., Dana, P. H., Mathur, V., Ocano, M., Hong, E. J., Wang, Y. E., Somaroo, S., Caffrey, B. E., Potluri, S., and Huang, E. S. (2007) PFAAT Version 2.0. A tool for editing, annotating, and analyzing multiple sequence alignments. *BMC Bioinformatics* **8**, 381
 27. Harris, R. K., and Mann, B. E. (eds) (1978) *NMR and the Periodic Table*, pp. 263–264, Academic Press, London
 28. Delaglio, F., Grzesiek, S., Vuister, G. W., Zhu, G., Pfeifer, J., and Bax, A. (1995) NMRPipe. A multidimensional spectral processing system based on UNIX pipes. *J. Biomol. NMR* **6**, 277–293
 29. Johnson, B. A., and Blevins, R. A. (1994) NMRView: A computer program for the visualization and analysis of NMR data. *J. Biomol. NMR* **4**, 603–614
 30. Mulder, F. A., Schipper, D., Bott, R., and Boelens, R. (1999) Altered flexibility in the substrate-binding site of related native and engineered high-alkaline *Bacillus subtilis*. *J. Mol. Biol.* **292**, 111–123
 31. Vitorino, M., Coin, F., Zlobinskaya, O., Atkinson, R. A., Moras, D., Egly, J. M., Poterszman, A., and Kieffer, B. (2007) Solution structure and self-association properties of the p8 TFIIF subunit responsible for trichothiodystrophy. *J. Mol. Biol.* **368**, 473–480
 32. Daragan, V. A., and Mayo, K. H. (1997) Motional model analyses of protein and peptide dynamics using ¹³C and ¹⁵N NMR relaxation. *Prog. NMR Spectrosc.* **31**, 63–105
 33. Cavanagh, J., Fairbrother, W., Palmer, A., 3rd, Skelton, N., and Rance, M. (2006) *Protein NMR Spectroscopy: Principles & Practice*, 2nd Ed., Academic Press Inc., San Diego
 34. Cornilescu, G., Delaglio, F., and Bax, A. (1999) Protein backbone angle restraints from searching a database for chemical shift and sequence homology. *J. Biomol. NMR* **13**, 289–302
 35. Güntert, P., Mumenthaler, C., and Wüthrich, K. (1997) Torsion angle dynamics for NMR structure calculation with the new program DYANA. *J. Mol. Biol.* **273**, 283–298
 36. Herrmann, T., Güntert, P., and Wüthrich, K. (2002) Protein NMR structure determination with automated NOE assignment using the new software CANDID and the torsion angle dynamics algorithm DYANA. *J. Mol. Biol.* **319**, 209–227
 37. Hanzawa, H., de Ruwe, M. J., Albert, T. K., van Der Vliet, P. C., Timmers, H. T., and Boelens, R. (2001) The structure of the C4C4 ring finger of human NOT4 reveals features distinct from those of C3HC4 RING fingers. *J. Biol. Chem.* **276**, 10185–10190
 38. Hoof, R. W., Vriend, G., Sander, C., and Abola, E. E. (1996) Errors in protein structures. *Nature* **381**, 272
 39. Laskowski, R. A., Rullmann, J. A., MacArthur, M. W., Kaptein, R., and Thornton, J. M. (1996) AQUA and PROCHECK-NMR. Programs for checking the quality of protein structures solved by NMR. *J. Biomol. NMR* **8**, 477–486
 40. Stoilov, P., Rafalska, I., and Stamm, S. (2002) YTH. A new domain in nuclear proteins. *Trends Biochem. Sci.* **27**, 495–497
 41. Zhang, Z., Theler, D., Kaminska, K. H., Hiller, M., de la Grange, P., Pudimat, R., Rafalska, I., Heinrich, B., Bujnicki, J. M., Allain, F. H., and Stamm, S. (2010) The YTH domain is a novel RNA binding domain. *J. Biol. Chem.* **285**, 14701–14710
 42. Deshaies, R. J., and Joazeiro, C. A. (2009) RING domain E3 ubiquitin ligases. *Annu. Rev. Biochem.* **78**, 399–434
 43. Dudev, T., Lin, Y. L., Dudev, M., and Lim, C. (2003) First-second shell interactions in metal-binding sites in proteins. a PDB survey and DFT/

Solution Structure of RING Finger-like Domain of RBBP6

- CDM calculations. *J. Am. Chem. Soc.* **125**, 3168–3180
44. Kay, L. E., Torchia, D. A., and Bax, A. (1989) Backbone dynamics of proteins as studied by ^{15}N inverse detected heteronuclear NMR spectroscopy. Application to staphylococcal nuclease. *Biochemistry* **28**, 8972–8979
45. Dudev, T., and Lim, C. (2002) Factors governing the protonation state of cysteines in proteins. An *ab initio*/CDM study. *J. Am. Chem. Soc.* **124**, 6759–6766
46. Bombarda, E., Morellet, N., Cherradi, H., Spiess, B., Bouaziz, S., Grell, E., Roques, B. P., and Mély, Y. (2001) Determination of the $\text{p}K_a$ of the four Zn^{2+} -coordinating residues of the distal finger motif of the HIV-1 nucleocapsid protein. Consequences on the binding of Zn^{2+} . *J. Mol. Biol.* **310**, 659–672
47. Goodfellow, B. J., Lima, M. J. O., Ascenso, C., Kennedy, M., Sikkink, R., Rusnak, F., Moura, I., and Moura, J. J. (1998) The use of ^{113}Cd NMR chemical shifts as a structural probe in tetrathiolate metalloproteins. *Inorg. Chim. Acta* **273**, 279–287
48. Atkinson, R. A., and Bruno, K. (2004) *Prog. NMR Spectrosc.* **44**, 141–187
49. Dominguez, C., Boelens, R., and Bonvin, A. M. (2003) HADDOCK. A protein-protein docking approach based on biochemical or biophysical information. *J. Am. Chem. Soc.* **125**, 1731–1737
50. Holm, L., and Sander, C. (1993) Protein structure comparison by alignment of distance matrices. *J. Mol. Biol.* **233**, 123–138
51. Buchwald, G., van der Stoep, P., Weichenrieder, O., Perrakis, A., van Lohuizen, M., and Sixma, T. K. (2006) Structure and E3-ligase activity of the Ring-Ring complex of polycomb proteins Bmi1 and Ring1b. *EMBO J.* **25**, 2465–2474
52. Zhang, M., Windheim, M., Roe, S. M., Pegg, M., Cohen, P., Prodromou, C., and Pearl, L. H. (2005) Chaperoned ubiquitylation. Crystal structures of the CHIP U box E3 ubiquitin ligase and a CHIP-Ubc13-Uev1a complex. *Mol. Cell* **20**, 525–538
53. Xu, Z., Devlin, K. I., Ford, M. G., Nix, J. C., Qin, J., and Misra, S. (2006) Structure and interactions of the helical and U-box domains of CHIP, the C terminus of HSP70 interacting protein. *Biochemistry* **45**, 4749–4759
54. Andersen, P., Kragelund, B. B., Olsen, A. N., Larsen, F. H., Chua, N. H., Poulsen, F. M., and Skriver, K. (2004) Structure and biochemical function of a prototypical *Arabidopsis* U-box domain. *J. Biol. Chem.* **279**, 40053–40061
55. Chou, C. C., Forouhar, F., Yeh, Y. H., Shr, H. L., Wang, C., and Hsiao, C. D. (2003) Crystal structure of the C-terminal 10-kDa subdomain of Hsc70. *J. Biol. Chem.* **278**, 30311–30316
56. Wan, T., Zhou, X., Chen, G., An, H., Chen, T., Zhang, W., Liu, S., Jiang, Y., Yang, F., Wu, Y., and Cao, X. (2004) Novel heat shock protein Hsp70L1 activates dendritic cells and acts as a Th1 polarizing adjuvant. *Blood* **103**, 1747–1754
57. Houben, K., Wasielewski, E., Dominguez, C., Kellenberger, E., Atkinson, R. A., Timmers, H. T., Kieffer, B., and Boelens, R. (2005) Dynamics and metal exchange properties of C4C4 RING domains from CNOT4 and the p44 subunit of TFIIF. *J. Mol. Biol.* **349**, 621–637
58. Nordquist, K. A., Dimitrova, Y. N., Brzovic, P. S., Ridenour, W. B., Munro, K. A., Soss, S. E., Caprioli, R. M., Klevit, R. E., and Chazin, W. J. (2010) Structural and functional characterization of the monomeric U-box domain from E4B. *Biochemistry* **49**, 347–355
59. Vander Kooi, C. W., Ohi, M. D., Rosenberg, J. A., Oldham, M. L., Newcomer, M. E., Gould, K. L., and Chazin, W. J. (2006) The Prp19 U-box crystal structure suggests a common dimeric architecture for a class of oligomeric E3 ubiquitin ligases. *Biochemistry* **45**, 121–130
60. Brzovic, P. S., Keeffe, J. R., Nishikawa, H., Miyamoto, K., Fox, D., 3rd, Fukuda, M., Ohta, T., and Klevit, R. (2003) Binding and recognition in the assembly of an active BRCA1/BARD1 ubiquitin-ligase complex. *Proc. Natl. Acad. Sci. U.S.A.* **100**, 5646–5651
61. Xu, Z., Kohli, E., Devlin, K. I., Bold, M., Nix, J. C., and Misra, S. (2008) Interactions between the quality control ubiquitin ligase CHIP and ubiquitin conjugating enzymes. *BMC Struct. Biol.* **8**, 26